BJA

British Journal of Anaesthesia, 120 (4): 745–760 (2018)

doi: 10.1016/j.bja.2017.12.033
Advance Access Publication Date: 15 February 2018
Neuroscience and Neuroanaesthesia

NEUROSCIENCE AND NEUROANAESTHESIA

Inhibition of RhoA reduces propofol-mediated growth cone collapse, axonal transport impairment, loss of synaptic connectivity, and behavioural deficits

M. L. Pearn[1,2,10], J. M. Schilling[1,2,10], M. Jian[1,2,5], J. Egawa[1,2], C. Wu[3], C. D. Mandyam[1,2], M. J. Fannon-Pavlich[1,2], U. Nguyen[1,2], J. Bertoglio[6], M. Kodama[1,2,4,7], S. K. Mahata[4], C. DerMardirossian[8,9], B. P. Lemkuil[2], R. Han[5], W. C. Mobley[3], H. H. Patel[1,2], P. M. Patel[1,2] and B. P. Head[1,2,*]

[1]Veterans Affairs San Diego Healthcare System, UCSD, San Diego CA, USA, [2]Department of Anesthesiology, UCSD, San Diego, CA, USA, [3]Department of Neurosciences, UCSD, San Diego, CA, USA, [4]Metabolic Physiology and Ultrastructural Biology Laboratory, UCSD, San Diego CA, USA, [5]Department of Anesthesiology, Beijing Tiantan Hospital, Capital Medical University, Beijing, China, [6]INSERM U749, Institut Gustave Roussy, Universite Paris-sud, Paris, France, [7]Department of Anesthesiology, National Defense Medical College, Tokorozawa, Saitama, Japan, [8]Department of Immunology and Microbial Sciences, TSRI, La Jolla, CA, USA and [9]Department of Cell and Molecular Biology, TSRI, La Jolla, CA, USA

*Corresponding author. E-mail: bhead@ucsd.edu.

[10] Pearn and Schilling share equal first authorship.

Abstract

Background: Exposure of the developing brain to propofol results in cognitive deficits. Recent data suggest that inhibition of neuronal apoptosis does not prevent cognitive defects, suggesting mechanisms other than neuronal apoptosis play a role in anaesthetic neurotoxicity. Proper neuronal growth during development is dependent upon growth cone morphology and axonal transport. Propofol modulates actin dynamics in developing neurones, causes RhoA-dependent depolymerisation of actin, and reduces dendritic spines and synapses. We hypothesised that RhoA inhibition prevents synaptic loss and subsequent cognitive deficits. The present study tested whether RhoA inhibition with the botulinum toxin C3 (TAT-C3) prevents propofol-induced synapse and neurite loss, and preserves cognitive function.
Methods: RhoA activation, growth cone morphology, and axonal transport were measured in neonatal rat neurones (5–7 days *in vitro*) exposed to propofol. Synapse counts (electron microscopy), dendritic arborisation (Golgi–Cox), and network connectivity were measured in mice (age 28 days) previously exposed to propofol at postnatal day 5–7. Memory was assessed in adult mice (age 3 months) previously exposed to propofol at postnatal day 5–7.
Results: Propofol increased RhoA activation, collapsed growth cones, and impaired retrograde axonal transport of quantum dot-labelled brain-derived neurotrophic factor, all of which were prevented with TAT-C3. Adult mice previously treated with propofol had decreased numbers of total hippocampal synapses and presynaptic vesicles, reduced hippocampal dendritic arborisation, and infrapyramidal mossy fibres. These mice also exhibited decreased hippocampal-

Editorial decision: December 26, 2017; **Accepted:** December 26, 2017

dependent contextual fear memory recall. All anatomical and behavioural changes were prevented with TAT-C3 pre-treatment.
Conclusion: Inhibition of RhoA prevents propofol-mediated hippocampal neurotoxicity and associated cognitive deficits.

Keywords: axonal transport; growth cone; hippocampus; infrapyramidal; synapses

Editor's key points

- In previous studies, propofol modulates actin dynamics in developing neurones via RhoA-dependent depolymerisation of actin.
- Combined *in vitro* and *in vivo* experiments in mice showed that RhoA inhibition prevented propofol-induced synapse and neurite loss and preserved cognitive function.
- RhoA activation is a potential target for prevention propofol-induced neurotoxicity.

Anaesthetic exposure during the period of synaptogenesis in the developing brain causes widespread neurodegeneration and long-term cognitive deficits.[1–7] The spectrum of anaesthetic neurotoxicity in rodent models includes apoptosis of neurones, glia and oligodendroglia, aberrant cell cycle entry, dendritic spine and synapse loss, remodelling of the actin cytoskeleton in glia, abnormalities of mitochondrial fission, fusion, and function, and epigenetic changes that might reduce neuronal plasticity. Moreover, anaesthetic neurotoxicity in the form of apoptosis occurs not only in rodents, but also in subhuman primates. In all experimental animal models, anaesthetic-induced cognitive dysfunction appears long lasting (i.e. seen a year after anaesthesia exposure in nonhuman primates) and hippocampal in nature (i.e. affecting learning and memory). Anaesthetic neurotoxicity is a robust finding demonstrated by a number of laboratories, in a number of species of experimental animals, and with widely varying experimental protocols.

Many studies investigating anaesthetic-mediated toxicity have focused on neuronal apoptosis.[1–4,6,8–17] A number of lines of evidence, however, indicate that preventing apoptotic cell death does not reliably ameliorate anaesthetic-induced cognitive deficits.[5,18] The extent of apoptosis has been estimated to be approximately 1–2% of neurones in the cortex[19]; however, a persistent reduction in neurone number has not been reported. By contrast, there is a 50% synapse loss immediately after anaesthetic exposure in the hippocampus, and a reduction in synapse number of 10% occurs 3 months after exposure.[7] Furthermore, neuronal apoptosis occurs to a similar extent in male and female rodent pups.[20] We have shown that TAT-Pep5, a peptide that inhibits $p75^{NTR}$ mediated RhoA activation,[11] prevents isoflurane-induced apoptosis.[12] However, TAT-Pep5 administration does not ameliorate cognitive deficits.[21] Collectively, these data demonstrate that factors other than apoptosis also contribute to anaesthetic neurotoxicity and anaesthetic-induced cognitive dysfunction.

Cognitive capacity is contingent upon proper neuronal network development, which depends on proper neuronal migration, synapse formation, and network connectivity during brain development.[22–25] Neurite extension and migration is facilitated by growth cone advancement towards appropriate targets in order to establish functional circuits.[23,25] This neuronal path finding relies upon actin-dependent events, which include growth cone motility and axonal transport of neurotrophins [i.e. nerve growth factor and brain-derived neurotrophic factor (BDNF)] from nerve terminals back to the cell body and *vice versa*.[22–25] Disruption of growth cone morphology (via actin dysregulation) or impaired axonal transport leads to aberrant connectivity and impaired cognition.[23,26–30]

Actin dynamics are regulated by Rho GTPases (RhoA, Rac1, and Cdc42), small G proteins that activate/deactivate downstream effector proteins.[23,26,31] RhoA activation results in actin stress fibre formation, growth cone collapse, and impaired axonal transport; Rac1 and Cdc42 activation facilitates lamellipodia and filopodia formation, growth cone protrusion, and axonal transport.[23,27,31] The timing and balance of Rho GTPase activation is critical and necessary for proper neuronal targeting and synapse formation during the critical periods of network formation.[23,32] Dysfunctional Rho GTPase signalling results in altered actin dynamics and loss of or aberrant neuronal connectivity and cognitive dysfunction.[23,26,27,31,33,34]

We have shown that anaesthetic exposure of neonatal neurones alters Rho GTPase activity and neurite actin dynamics.[11–13] Given that regulation of actin dynamics plays an important role in neuronal pathfinding, circuit formation, and brain development,[23,26,27,31,33,34] and that propofol alters Rho GTPase signalling,[11–13] we tested the hypothesis that propofol causes neurotoxicity through increased RhoA activation, actin dysregulation, growth cone collapse, impaired axonal transport, and altered neuronal connectivity, all of which lead to cognitive deficits.

Methods

Preparation of neuronal cell cultures

All studies performed on animals were approved by Veteran Affairs San Diego Institutional Animal Care and Use Committee (San Diego, CA, USA) and conform to the guidelines of Public Health Service Policy on Human Care and Use of Laboratory Animals. Embryonic rat neurones (Sprague Dawley; Harlan Laboratories, Inc., Indianapolis, IN, USA) were isolated as described.[35] In brief, hippocampal neurones isolated from rat pups at embryonic age 16–18 were plated on poly-L-lysine coated coverslips in culture plates or within microfluidic chambers (Xona Microfluidics, Temecula, CA, USA). Axons from hippocampal neurones entered the microfluidic chamber microgroove at 3 days *in vitro* (DIV) and reached the distal axon compartments between 5–7 DIV. During neurone culture maintenance, half the media was removed and replaced with fresh maintenance media every 24–48 h.

Anaesthetic neurotoxicity model *in vitro*

Primary neuronal cultures (DIV 5–7) were placed in an incubator and exposed to 3 μM propofol (2,6-diisopropylphenol;

Sigma, St Louis, MO, USA) and then placed in an incubator for 2 h in a gas mixture of 5% CO_2, 21% O_2, and 74% nitrogen at a flow rate of 2 litres min^{-1}. Temperature was maintained at 37°C. A subset of neurones was pre-treated with 50 μg ml^{-1} of the RhoA inhibitor TAT-C3 for 2 h before propofol exposure.

To make vehicle control solution, DMSO was diluted to 0.1% in Neurobasal media. Propofol 3uM solution was made by serial dilution in stock DMSO followed by Neurobasal media (final concentration: 3uM propofol in DMSO 0.1%).

Axonal transport of quantum dot-labelled mature BDNF

Neurones (DIV 5–7) were prepared for live imaging of quantum dot (QD)-labelled mature BDNF transport as described.[35] Before live imaging of QD-BDNF transport, microfluidic compartments were depleted of BDNF by rinsing with BDNF-free, serum free Neurobasal® Media (Thermo Fisher Scientific, Waltham, MA, USA) every 30 min for 2 h. Mono-biotinylated brain derived neurotrophic factor was generated as described.[36] QD 655 streptavidin conjugate was purchased from Life Technologies (Life Technologies, San Diego, CA, USA). To prepare the QD-BDNF conjugates, 50 nM mono-biotinylated BDNF dimer was mixed with 50 nM QD 655-streptavidin conjugates in Neurobasal® Media and incubated on ice for 1 h. After 1 h incubation, the QD-BDNF was diluted in Neurobasal® Media to a final concentration of 0.25 nM. QD-BDNF (0.25 nM) was added to the distal axonal compartments of the microfluidic chambers for 2 h at 37°C. QD-BDNF is taken up into neurones by TrkB receptor binding and endocytosis. After 2 h incubation with QD-BDNF and before imaging, distal axonal compartments were rinsed three times with Neurobasal® Media to wash off any unbound QD-BDNF. Live QD-BDNF transport was captured with an inverted immunofluorescence microscope system (Leica, Buffalo Grove, IL, USA) using a 100× oil objective with a Charged coupled device (CCD) camera (Rolero-MGi Fast 1397; Qimaging, Surrey, British Columbia, Canada) and environmental chamber to maintain constant temperature (37°C) and CO_2 (5%). The QD 655 signal was seen using Texas red excitation/emission cubes. Live images of QD-BDNF transport were captured within the middle axons at a camera speed of 1 frame s^{-1} for 2 min. Kymographs were generated and analysed using MetaMorph Software (Molecular Devices, Sunnyvale, CA, USA). Statistical analysis was performed using Prism 7 (GraphPad Software, La Jolla, CA, USA). Sample size (n) equals the number of QD-BDNF dimers counted per experimental condition.

Protein extraction and immunoblot analysis

Protein lysates were separated by sodium dodecyl sulphate–polyacrylamide gel electrophoresis using 4–12% or 10% acrylamide gels (Invitrogen, Carlsbad, CA, USA) and transferred to polyvinylidene difluoride membranes (Millipore, Billerica, MA, USA) by electroelution. Membranes were blocked in 20 mM phosphate-buffered saline (PBS)/Tween (1%) containing 3% bovine serum albumin (BSA) and incubated with primary antibody overnight at 4°C. Primary antibodies were seen using secondary antibodies conjugated to horseradish peroxidase (Santa Cruz Biotech, Santa Cruz, CA, USA) and chemiluminescent reagent (Lumigen, Southfield, MI, USA). Image J software (National Institutes of Health, Bethesda, MD, USA) was used for densitometry analysis as described.[11]

Neurone staining and immunofluorescence microscopy

Neurones (DIV 5–7) were prepared for immunofluorescence microscopy as described.[11–13] Primary neurones were fixed with 4% paraformaldehyde in PBS for 10 min at room temperature, incubated with 100 mM glycine (pH 7.4) for 10 min to quench aldehyde groups, permeabilised in buffered 0.1% Triton X-100 for 10 min, blocked with 1% BSA/PBS/Tween (0.05%) for 20 min and then incubated with primary antibodies (1:100) in 1% BSA/PBS/Tween (0.05%) for 24–48 h at 4°C. Excess antibody was removed by washing with PBS/Tween (0.1%) for 15 min followed by incubation with Alexa-conjugated secondary antibody (1:250) for 1 h. To remove excess secondary antibody, neurones were washed six times at 5 min intervals with PBS/Tween (0.1%) and incubated for 20 min with the nuclear stain 4′,6-diamidino-2-phenylindole (DAPI) diluted 1:5000 in PBS. RhoA-GTP primary antibody staining (NewEast Biosciences, King of Prussia, PA, USA) normalised to nuclear DAPI staining was utilised to assay RhoA activation. Phalloidin staining was used to assess growth cone area. Neurones were washed for 10 min with PBS and left in PBS for imaging. As described,[37] deconvolution images were captured at 100× magnification using a DeltaVision deconvolution microscope system (Applied Precision, LLC, Issaquah, WA, USA). This system includes a Photometrics CCD camera mounted on a Nikon TE-200 inverted epifluorescence microscope. Exposure times were set such that the camera response was in the linear range for each fluorophore. Maximal projection volume views or single optical sections were seen. Pixels were assessed quantitatively by CoLocalizer Pro software (Colocalization Research Software, Japan). Neuronal growth cone area was assessed by Aperio ScanScope software (Leica, Buffalo Grove, IL, USA). Differential interference contrast (DIC) images were also captured to assure that any change in phalloidin staining was secondary to growth cone collapse and not a change in the concentration of F-actin alone. Statistical analysis was performed using Prism 6 (GraphPad Software, San Diego, CA, USA).

Anaesthetic neurotoxicity model *in vivo*

Postnatal day 5–7 (PND 5–7) wild type (WT) male C57BL/6 mice were separated from their dams and placed in a temperature-controlled incubator set to 37°C. Animals were randomised into four groups (n=5 per group). Mice were given a single intraperitoneal (i.p.) injection of propofol or Intralipid (50 mg kg^{-1}) followed by two i.p. injections of propofol or Intralipid (25 mg kg^{-1}) at 2 h intervals, totalling 6 h of exposure. Before propofol exposure, mice were pre-treated with either TAT-MUT (control) or TAT-C3 (12.5 mg kg^{-1}, i.p.) for 2 h. Pups were allowed to recover in the incubator for 2 h after the final injection and returned to their dams. Mice were sacrificed 4 weeks after propofol exposure and brains were prepared for further analysis. For behavioural studies, a total of 54 mice were investigated at age 3 months after anaesthetic exposure.

Histological preparation for microscopy

Under deep pentobarbital anaesthesia, a midline thoracotomy was performed on 4-week-old mice, and the descending thoracic aorta was occluded. A 20 gauge needle was inserted into the left ventricle and the animal was perfused transcardially with 20 ml of heparinised saline followed by 20 ml of 4% buffered formalin fixative. The right atrium was incised to

permit free flow of perfusion fluid. The brain was removed and post-fixed for 24–48 h in fixative. Brains were placed in sucrose (30% in PBS with 0.01% sodium azide) followed by cryostat sectioning (40 μm) and preparation for immunofluorescence microscopy. Hippocampal sections were stained with primary antibody overnight at room temperature followed by secondary antibody conjugated to Alexa 488, 594. or 647 for 1 h at room temperature. Immunostaining was seen by fluorescent tyramide signal amplification (1:50, Molecular Probes. Sections were co-stained with the nuclear stain DAPI (1:3000, Life Technologies). Confocal images were captured using a Nikon A1R confocal system (Melville, NY) using 4× and 20× objectives. Between 30 and 80 optical sections of approximately 0.1–0.3 μm were captured. Exposure times were such that the camera response was in the linear range for each fluorophore.

Golgi–Cox impregnation

Mice (age 4 weeks) were killed by decapitation after deep 5% isoflurane anaesthesia, and the brain was quickly removed and submerged in Golgi–Cox solution A + B (FD Neurotechnologies Inc., Columbia, MD, USA) for 8 days, followed by solution C for 4 days at room temperature and stored at −80°C until processed. Frozen brain tissue was cut coronally on a cryostat at 80-μm-thick sections and stained with solution D + E and dehydrated according to the manufacturer's instructions. To evaluate hippocampal neurone morphology, a Zeiss AxioImager microscope and a computer-based system (Neurolucida; MBF Bioscience, Williston, VT, USA) were used to generate three-dimensional neurone tracings that were seen and analysed using NeuroExplorer (MBF Bioscience).

Electron microscopy

Mice (age 4 weeks) were transcardially perfused and brain tissue was fixed with standard Karnovsky's fixative, 4% paraformaldehyde, 1% gluteraldehyde, 0.1 M cacodylate buffer with 5 mM $CaCl_2$. Hippocampi were dissected from whole brain after 24 h and 400 μm vibratome slices prepared and re-fixed for an additional 24 h. Brains were blocked to include hippocampal areas, one hemisphere for sagittal orientation, and one hemisphere for coronal. Blocks were re-fixed for an additional 24 h followed by post-fixation with 1% OsO_4 in 0.1 M cacodylate buffer, *en bloc* stained with uranyl acetate and embedded with flat orientation to locate appropriate hippocampal regions of interest. Each block was thick sectioned, stained with toluidine blue, and re-trimmed to isolate hippocampal areas before preparation of grids. Grids (70 nm sections) were stained with uranyl acetate and lead nitrate for contrast and observed on an electron microscope (1200 EX-II; JEOL, Tokyo, Japan) equipped with a digital camera system. Twenty-five random low magnification (2500×) micrographs and 50 high magnification (15 000×) micrographs of the CA3 region were obtained from each specimen. Total numbers of synapses and presynaptic vesicles were measured as described.[38]

Behavioural analysis

Fear conditioning was performed on adult mice (age 3 months) exposed to propofol at postnatal day 5–7 as described.[39] In brief, we used four acrylic chambers (30 cm wide × 20 cm deep × 19 cm high; Med Associates Inc., St Albans, VT, USA) placed in sound attenuating boxes, and foot shocks delivered through the floor consisting of 36 stainless steel rods wired to a shock generator. A computer controlled presentation of unconditioned stimuli (US: scrambled foot shock) and conditioned stimuli (CS: auditory tone), and real-time video recordings continuously monitored animal movements. Freezing was determined using Video Freeze Software (Med Associates Inc., ANY-MAZE, San Diego Instruments, San Diego, CA, USA). After an acclimation period (2 min), mice were presented with a tone (CS: 90 dB, 5 kHz) for 30 s that co-terminated with a foot shock (US: 2.0 s, 1.0 mA) in dark chambers. A total of three tone-shock pairings were presented with a varying inter-trial interval of 30–90 s. Freezing time was measured during each CS to determine fear acquisition level across groups. Context fear was tested 24 h later. Cued fear was tested 24 h after context fear. To remove contextual cues, chambers were altered across several dimensions (odour: scent; visual: light chambers and walls via plastic inserts; tactile: new floor covering) to minimise generalisation from the conditioning context. The session started with a 3 min acclimation period, during which no tones were presented ('pre-tone' period), then 10 blocks of five CS were presented for 30 s each with an inter-trial interval of 5 s. Freezing was recorded during each CS. For analysis, total freezing time was averaged as total freezing during all CS presentations.

Statistical analysis

Data were analysed using GraphPad Prism 7 and IBM SPSS Statistics v24 (IBM Corporation, Armonk, NY, USA). After testing distribution with Shapiro–Wilk's test for normality, we performed either unpaired Student's *t*-test, Mann–Whitney *U*-test, one-way analysis of variance (ANOVA), or Kruskal–Wallis test followed by appropriate *post hoc* tests and Holm–Sidak correction for multiple comparisons. ANOVA or contingency table analysis followed by appropriate *post hoc* tests and Holm–Sidak correction for multiple comparisons was used when multiple factors (e.g. 'drug treatment', 'peptide', 'time') were analysed. For behavioural analysis, mice were randomised to treatment and investigated by a blinded observer. Statistical analysis was performed with coded groups first by an observer blinded to treatment. A *post hoc* power analysis was performed with G*Power 3.1 (Düsseldorf, Germany) (PMID: 17695343). Data are presented as mean (SEM) or median where appropriate. All graphs present data as mean (SEM). Statistical significance was assumed for $\alpha<0.05$.

Results

Propofol increases RhoA activation, causes growth cone collapse, and impairs retrograde axonal transport of BDNF in primary hippocampal rat neurones

Previous work from our laboratory showed that p75 neurotrophin receptor ($p75^{NTR}$) activation is a contributing factor in propofol-mediated neurotoxicity.[11–13] Because $p75^{NTR}$ activates RhoA, we hypothesised that propofol exposure of neonatal neurones increases RhoA-GTP (activated RhoA), resulting in growth cone collapse and impaired retrograde axonal transport of BDNF. Neurones (DIV 5–7) grown in microfluidic chambers were exposed to propofol (3 μM, 15 min, and 4 h) or X% dimethylsulphoxide (DMSO; control). Propofol exposure resulted in increased expression of RhoA-GTP compared with control [Fig. 1a; propofol, 3.5 (0.4) X, $n=18$ compared with control 2.2 (0.4) X, $n=13$, $t(29)=2.24$, $P=0.03$]. F-

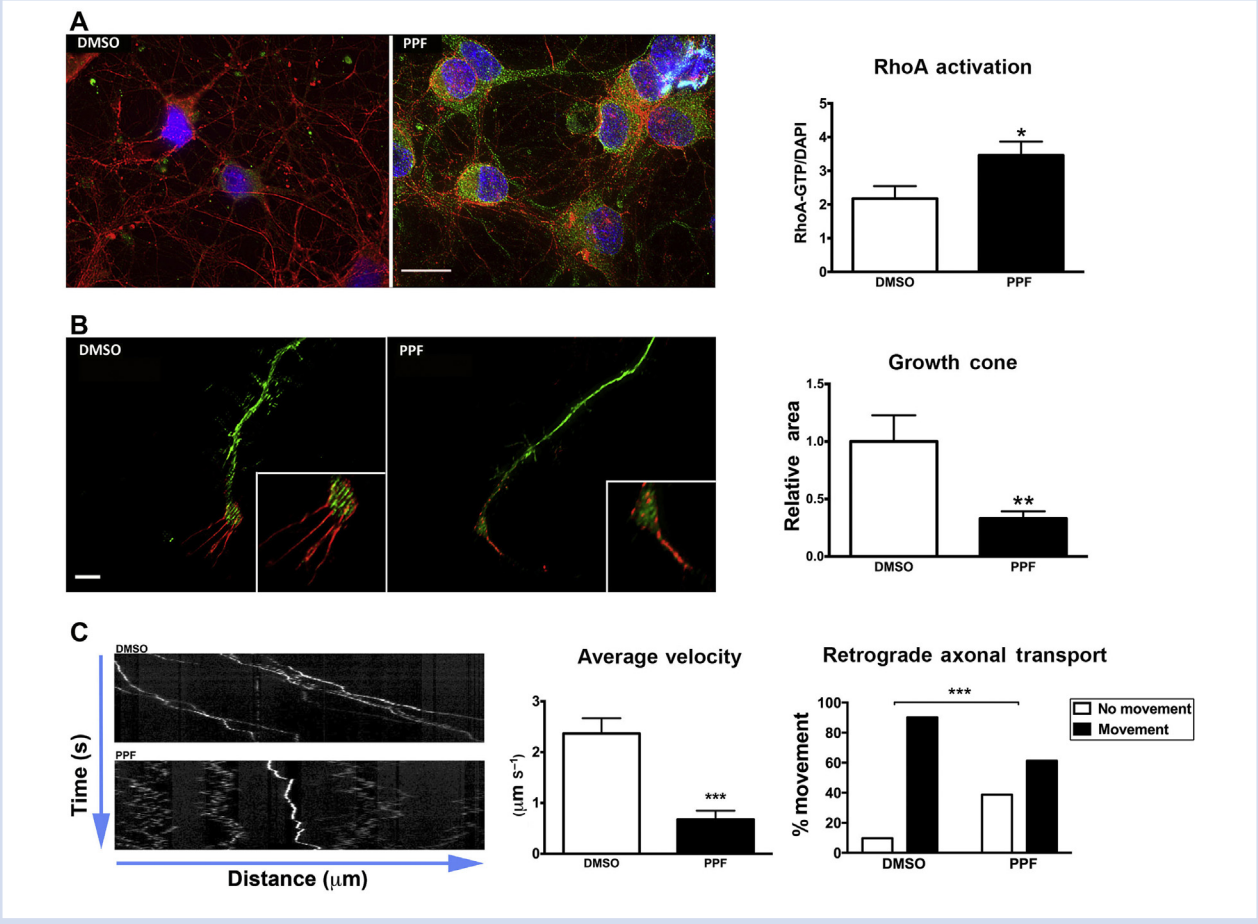

Fig 1. Primary neurones exposed to propofol (PPF) show RhoA activation, growth cone collapse, and impaired retrograde axonal transport of quantum dot (QD)-labelled brain-derived neurotrophic factor (BDNF). Neurones were exposed to PPF (3 μM) for (a) 15 min or (b,c) 2 h in 5% CO_2 in air. (a) RhoA activation is indicated by RhoA-GTP immunofluorescence microscopy (green). Actin was stained with phalloidin (red) and nucleus was stained with DAPI (blue). RhoA-GTP is increased in neurones exposed to PPF *vs* DMSO (control). Quantitation of data is represented in the graph (n=13–18; *P=0.03). (b) Growth cone area was evaluated using phalloidin (red). Microtubules were stained for tau protein (green). Microscopy shows a decrease in growth cone area in neurones exposed to PPF *vs* DMSO (control). Quantitation of the data is represented in the graph (n=8–10; **P=0.002). (c) Retrograde axonal transport of BDNF was evaluated by live imaging of QD-BDNF. Representative kymographs are shown for neurones (*in vitro* days 5–7) exposed to either DMSO (top panel) or PPF (bottom panel). Retrograde movement is left to right. Individual QD-BDNF molecules are seen as a single line on the kymographs. More horizontal sloped lines represent processive movements of QD-BDNF along the axon, while more vertical sloped lines represent stationary, slower, or both QD-BDNF movements along the axon. Live imaging and kymograph analysis show a decrease in net average velocity and decrease in percent retrograde movement of QD-BDNF in neurones exposed to PPF. Quantitation of data is presented in the graphs. Average velocity (n=51–62; ***P<0.001). Percent movement (n=51–62; ***P<0.001). DAPI, 4′,6-diamidino-2-phenylindole; DMSO, dimethyl sulfoxide. Data are presented as mean (SEM); P was assumed significant when $\alpha < 0.05$; *P<0.05, **P<0.01, ***P<0.001.

actin staining (with phalloidin) showed that propofol exposure resulted in significantly decreased relative growth cone area compared with DMSO control [Fig. 1b; propofol median=0.25 X, n=10 compared with control median=0.89 X, n=8, U=7, P=0.002). Propofol exposure resulted in decreased average QD velocity [Supplementary material, Fig. 1 online video (DMSO) and Fig. 2 online video (Propofol); propofol median=0.19 μm s^{-1}, n=62 compared with control median 2.0 μm s^{-1}, n=51; U=744, P<0.001]. Retrograde axonal transport was scored as 'moving' or 'not moving' QD with results shown as percent net retrograde axonal movements of QD-BDNF labelled signalling endosomes compared with DMSO control (Fig. 1c). An association between treatment group (DMSO *vs* propofol) and QD movement [$\chi^2(1)$=12.26, P<0.001] with propofol treated neurones expressing a lower % QD movement compared with DMSO (61% *vs* 90%).

Supplementary data related to this article can be found online at https://doi.org/10.1016/j.bja.2017.12.033

TAT-C3 peptide attenuates propofol-induced growth cone collapse and retrograde axonal transport impairment of BDNF

We tested whether inhibition of RhoA activation by TAT-C3 reverses the deleterious effects of propofol. To test this hypothesis, DIV 5–7 neurones grown in microfluidic chambers

were pre-treated with TAT-C3 (50 μg ml^{-1}, 2 h) before propofol exposure. To confirm TAT-C3 inhibition of RhoA activity, we performed a mobility shift assay as described.[40] TAT-C3 (exoenzyme from *Clostridium botulinum*) inhibits RhoA by ADP ribosylation of asparagine 41 in the effector binding domain of the GTPase,[41] rendering it inactive; this modification increases the molecular weight (i.e. upward shift) of RhoA on immunoblot assay.[40] Lysates of neurones pre-treated with TAT-C3 for 2 h exhibited an upward shift of RhoA molecular weight, with no upward shift in Rac1 molecular weight, confirming the specificity of TAT-C3 inhibition for RhoA (Fig. 2a). We found a significant effect on relative growth cone area between treatment groups (n=4, P<0.001) with a significantly smaller growth cone area (phalloidin stain) after propofol exposure (mean rank=17.7, n=31) compared with DMSO control (mean rank =55.2, n=21, *vs* propofol, P<0.001) or neurones pre-treated with TAT-C3 before propofol exposure (mean rank =52.8, n=26, *vs* propofol, P<0.001; Fig. 2b). Average QD velocity (μm s^{-1}; Fig. 2c) was reduced by propofol (Supplementary material, Fig. 2 online video, mean rank=100.9, n=122) compared with DMSO (Supplementary material, Figure 1 online video, mean rank=181.6, n=65, P<0.001) and TAT-C3 propofol (Supplementary material, Fig. 3 online video, mean rank 167.5, n=96, P<0.001; H=55.3, P<0.001). QD analysis of retrograde axonal transport (Fig. 2c) indicated that QD movement was not distributed similarly across the different treatment groups [χ^2(2)=43.9, P<0.001] with propofol treated neurones (43%) showing the lowest % movement compared with DMSO (80%) and TAT-C3 propofol (82%). To look at group to group comparisons in more detail, corrected group to group comparisons

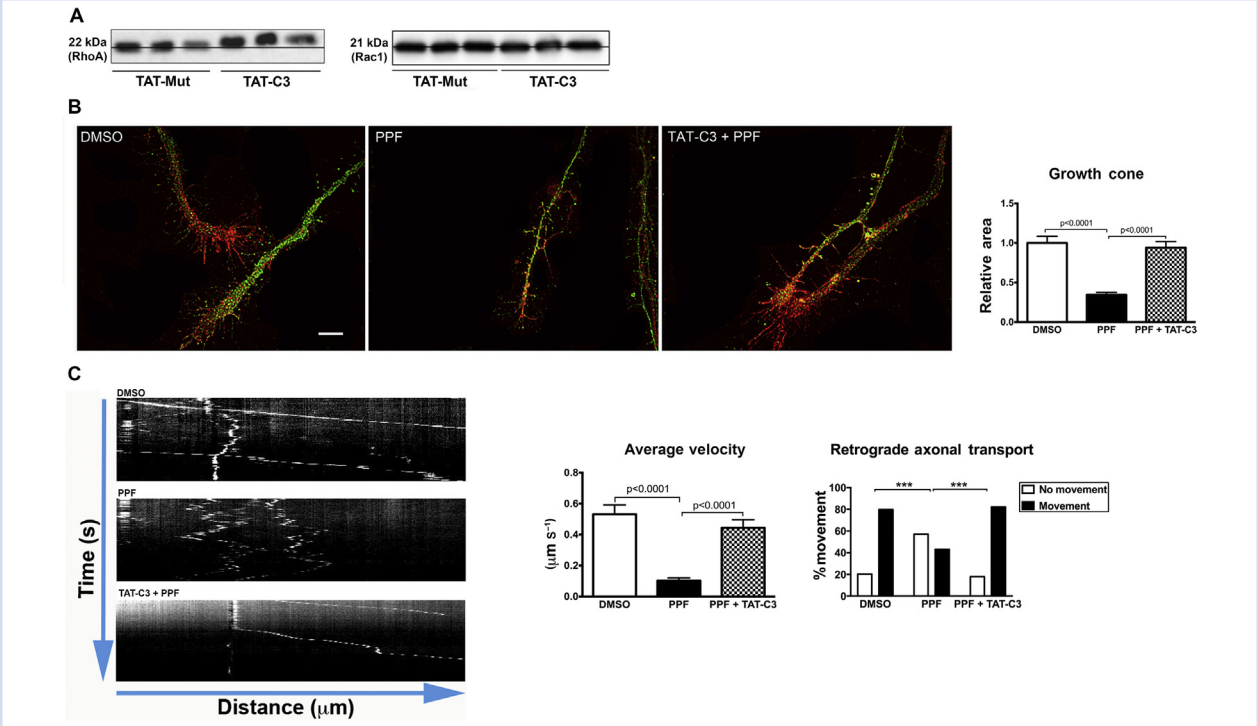

Fig 2. RhoA inhibitor TAT-C3 prevents propofol (PPF)-mediated growth cone collapse and impaired retrograde axonal transport of quantum dot (QD)-brain-derived neurotrophic factor (BDNF)-positive vesicles in neurones. Primary neurones were isolated from mouse brains at Embryonic day 16–18 and grown *in vitro* for 5–7 days. Neurones were then exposed to PPF (3 μM) for (b,c) 4 h. A subset of neurones was pre-treated with TAT-C3 (50 μg ml^{-1}, 2 h) 15 min before PPF exposure. (a) TAT-C3 inhibits RhoA activation by ADP ribosylation; this modification increases the molecular weight, causing an upward shift on immunoblot assay. Western blot analysis of whole cell lysates from primary neurones exposed to TAT-C3 (n=3) revealed an upward shift for RhoA treatment compared with TAT-Mut control (n=3; left immunoblot), indicative of RhoA-GDP[40]; TAT-C3 did not cause an upward shift in neuronal lysates probes for Rac1 (right immunoblot), confirming that TAT-C3 specifically inhibits RhoA and not other Rho GTPases. (b) Growth cone area was evaluated using phalloidin immunofluorescence microscopy (red). Microtubules were stained for τ (green). Microscopy shows a decrease in growth cone area in neurones exposed to PPF *vs* DMSO (control), an effect prevented with TAT-C3. Quantitation of data is represented in the graph (n=21–31; ***P<0.001). (c) Retrograde axonal transport of BDNF was evaluated by live imaging of quantum dot-labelled BDNF. Representative kymographs are shown for neurones (DIV 5–7) exposed to DMSO (top), or PPF (middle), or TAT-C3 plus PPF (bottom). Retrograde movement is left to right. Individual QD-BDNF molecules are seen as a single line on the kymographs. More horizontal sloped lines represent axonal movement of QD-BDNF-positive vesicles, while more vertical sloped lines represent stationary, of both impaired QD-BDNF movement. Live imaging and kymograph analysis shows a decrease in net average velocity and percent retrograde movement of QD-BDNF in neurones exposed to PPF. Neurones pre-treated with TAT-C3 before PPF exposure show both increased average velocity and percent retrograde movements compared with neurones exposed to PPF. Quantitation of data is presented in the graphs. Average velocity (n=65–122; ***P<0.001). Percent movement (n=64–121; ***P<0.001). DMSO, dimethyl sulfoxide; PPF, propofol; C3, TAT-C3; data are presented as mean (SEM); P was assumed significant when α<0.05; *P<0.05, **P<0.01, ***P<0.001.

were used [DMSO *vs* TAT-C3 propofol: $\chi^2(1)=0.15$, $P=0.70$; DMSO *vs* propofol: $\chi^2(1)=22.86$, $P<0.001$; propofol *vs* TAT-C3 propofol: $\chi^2(1)=34$, $P<0.001$]. Collectively, these data show that propofol-mediated growth cone collapse and impaired axonal transport occurs in part through RhoA activity, and can be reversed with TAT-C3 inhibition of RhoA activation.

Propofol exposure decreases infrapyramidal mossy fibre area in the hippocampus

Neuronal circuit formation during development is critical for long-term cognition. Neuronal pathfinding and circuit formation requires normal axonal transport of BDNF and growth cone morphology.[22–24,28,29,42–44] Because propofol exposure of neonatal neurones results in growth cone collapse (Fig. 1b) and impaired retrograde axonal transport of QD-BDNF (Fig. 1c) *in vitro*, we examined the effect of propofol on mossy fibre bundle formation in PND 5–7 mouse pups *in vivo* 28 days after propofol exposure. We investigated the mossy fibre bundles of the CA3 region of the hippocampus because its development requires proper axonal pathfinding, which is dependent on growth cone motility and axonal transport.[23,25,45–52] Additionally, synaptic connectivity that constitutes the mossy fibre bundle (dentate gyrus axons synapsing with CA3 dendrites) contributes substantially to learning and memory.[53–58] Synaptoporin antibody was used to stain and assess mossy fibre area within the infrapyramidal mossy fibre (IMF) and suprapyramidal mossy fibre (SMF)

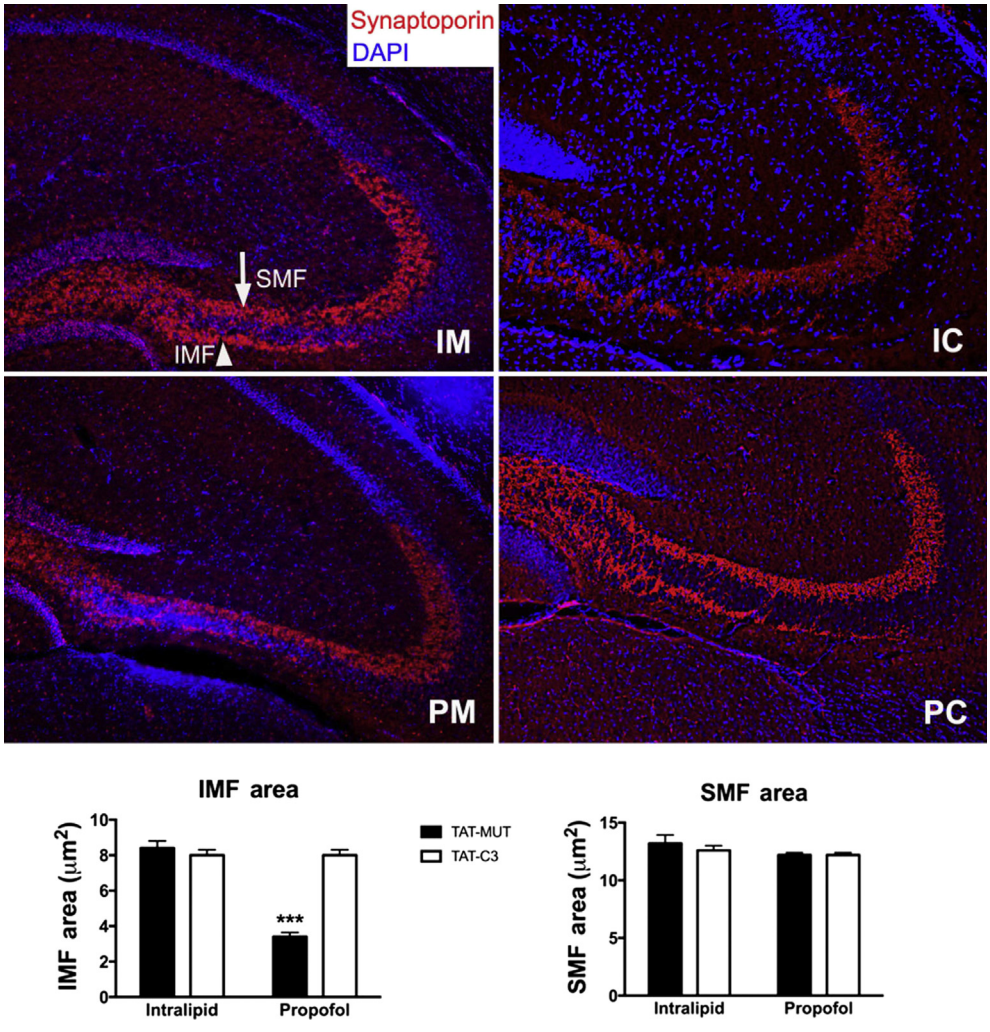

Fig 3. RhoA inhibition with TAT-C3 prevents propofol-mediated reduction of hippocampal infrapyramidal mossy fibre (IMF) area. Postnatal day 5–7 mice were pre-treated with TAT-MUT or TAT-C3 (12.5 mg kg^{-1} i.p., 2 h) and then exposed to propofol (50 mg kg^{-1}, 25 mg/kg, and 25 mg kg^{-1} i.p. injections separated by 2 h) or Intralipid (vehicle control). Four weeks after propofol exposure, hippocampal mossy fibre bundle area was evaluated using synaptoporin immunofluorescence microscopy (red). Nuclei were stained with DAPI (blue). Propofol exposure (PM, bottom left panel) significantly reduced IMF area ($n=5$, $P<0.001$), but not suprapyramidal mossy fibre (SMF) area (IM, top left panel) ($n=5$, $P=0.51$). Pre-treatment with TAT-C3 (PC, bottom right panel) preserved IMF area compared with propofol plus TAT-MUT (PM, bottom left panel; $n=5$, $P<0.001$). Arrow: SMF, arrow head: IMF. DAPI, 4′,6-diamidino-2-phenylindole; IC, Intralipid/TAT-C3; MF, mossy fibre; IM, Intralipid/TAT-mutant; i.p., intraperitoneal; PC, propofol/TAT-C3; PM, propofol/TAT-mutant. Quantitation of data is presented as mean (SEM); P was assumed significant when $\alpha < 0.05$; *$P<0.05$, **$P<0.01$, ***$P<0.001$.

bundles. Synaptoporin staining revealed that propofol exposure (indicated as PM in Fig. 3) significantly reduced area of the IMF bundle (Fig. 3: bottom right panel). The results of this analysis show a significant effect of propofol treatment [$F(1,16)=59.5$, $P<0.001$], peptide treatment [$F(1,16)=42$, $P<0.001$], and propofol by peptide interaction [$F(1,16)=59.5$, $P<0.001$]. Further, we looked at multiple comparisons and found a significant decrease of mossy fibre area in propofol/TAT-mut (PM) [$n=5$, 3.4 (0.2)] treated animals compared with IL/TAT-mut (IM) [$n=5$, 8.4 (0.4), $P<0.001$] and propofol/TAT-C3 (PC) [$n=5$, 8.0 (0.3), $P<0.001$]. The same analysis performed for the SMF bundle 28 days after single propofol exposure (6 h) did not reveal any significant effects. Taken together, the decrease in IMF area was significantly attenuated by TAT-C3 pre-treatment (indicated as PC in Fig. 3) before propofol exposure (Fig. 3: bottom right panel), while there was no effect on the SMF bundles.

Propofol exposure decreases dendritic branching and reduces total synapses in the hippocampus

The number of synapses in the hippocampus is influenced by the degree of dendritic branching. Dendritic branching is in part regulated by balanced Rho GTPases activity,[59–61] and by trophic support from synapsing axon terminals.[62–66] Increased RhoA activation decreases dendritic branching, leading to a decrease in synaptic contacts.[67–70] Because propofol activates RhoA (Fig. 1a) and decreases IMF bundle input toward the CA3 hippocampal region (Fig. 3), we examined the effects of propofol on dendritic branching and synaptic count in the hippocampus. PND 5–7 mouse pups were exposed to propofol for 6 h and sacrificed 28 days later to assess dendritic branching by Sholl analysis and synaptic count by electron microscopy.[39] For Sholl analysis, the apical dendrites of dentate gyrus granule cells and apical and basal dendrites of CA3 pyramidal neurones within the hippocampus were traced after Golgi–Cox staining. A representative example of a Golgi–Cox stained dentate gyrus granule cell is shown (Fig. 4a) along with neuronal tracings using Neurolucida software (Fig. 4b) and the corresponding 3D reconstruction with Sholl rings (Fig. 4c) from one animal. XYZ orientation of the cell in Fig. 4a and the corresponding depths of the cell shown are indicated in Fig. 4d. Fig. 4e shows representative granule cell tracings from each exposure group. Morphological analysis of granule cell apical dendrites demonstrated total number of dendritic intersections and distance from soma were significantly lower after propofol exposure (PM), while pre-treatment with TAT-C3 attenuated propofol-mediated dendritic retraction (Fig. 4f and g, respectively). We analysed Fig. 4f using a three-way ANOVA and found significant effects for the factors distance [$F(10,10)=343.5$, $P<0.001$], propofol [$F(1,10)=72.8$, $P<0.001$], and peptide [$F(1,10)=140.3$, $P<0.001$], in addition to the interactions between distance × propofol [$F(10,10)=18.4$, $P<0.001$], distance × peptide [$F(10,10)=7.5$, $P<0.001$], propofol × peptide [$F(1,10)=152.3$, $P<0.001$], and, most importantly distance × propofol × peptide [$F(10,10)=18.6$, $P<0.001$]. For the group to group comparisons at different distances from soma we found fewer intersections in the propofol/TAT-mut group compared with IL/TAT-MUT (from 70 μm to 150 μm, $P<0.05$) and propofol/TAT-C3 (from 50 μm to 150 μm, $P<0.05$). In Fig. 4f, we analysed the total number of intersections, with a significant effect of propofol treatment [$F(1,76)=21.38$, $P<0.001$], peptide treatment [$F(1,76)=23.57$, $P<0.001$] and propofol by peptide interaction [$F(1,76)=51.36$, $P<0.001$]. We found a significant decrease of dentate gyrus apical dendrites in propofol/TAT-MUT [$n=20$, 126 (6)] treated animals compared with IL/TAT-MUT [$n=20$, 177 (3), $P<0.001$] and propofol/TAT-C3 [$n=20$, 178 (0.3), $P<0.001$].

Fig. 4h shows representative CA3 pyramidal neurone tracings from each group (IM, IC, PM, PC). Total number of dendritic intersections and distance from soma in the apical dendrites of CA3 pyramidal neurones were significantly lower after propofol exposure (PM; Fig. 4i and j, respectively) and pre-treatment with TAT-C3 significantly attenuated propofol-mediated apical dendritic retraction of CA3 pyramidal neurones (Fig. 4i and j). We found (Fig. 4i) a significant effect for the factors distance [$F(10,10)=190.4$, $P<0.001$] and peptide [$F(1,10)=19.27$, $P<0.001$], while interactions were significant for propofol × peptide [$F(1,10)=8.03$, $P<0.01$] and distance × propofol × peptide [$F(10,10)=2.8$, $P<0.01$]. There was a significant decrease in number of intersections in the propofol/TAT-MUT group compared with IL/TAT-MUT (130 μm, $P<0.05$) and propofol/TAT-C3 (130 μm, $P<0.05$). The results of the soma-tip distance show a significant effect of peptide treatment [$F(1,76)=6.73$, $P=0.01$] and propofol by peptide interaction [$F(1,76)=14.36$, $P<0.001$]. *Post hoc* tests found a significant decrease of apical dendrites in propofol/TAT-MUT [$n=20$, 130 (4)] treated animals compared with IL/TAT-MUT [$n=20$, 155 7), $P<0.01$] and propofol/TAT-C3 [$n=20$, 162 (4), $P<0.001$]. In contrast, basal dendrites were unaffected by TAT-C3 pre-treatment with no significant difference between groups (Fig. 4i and j).

Synaptic count is influenced by Rho GTPase signalling and degree of dendritic branching.[71,72] Because propofol decreased dendritic branching via RhoA activation in both the dentate gyrus and CA3 granule cell apical dendrites of the hippocampus, we investigated the effect of propofol on synapses using electron microscopy. Synapses and presynaptic vesicles are visible in the representative control images under low magnification (2500×; Fig. 4k). Compared with control (Intralipid) exposed mouse pups (IM), propofol (PM) exposure reduced total synapse number (Fig. 4k and l). This reduction was attenuated by pre-treatment with TAT-C3 (PC; Fig. 4k and l) with a significant effect of propofol treatment [$F(1,56)=183.7$, $P<0.001$], peptide treatment [$F(1,56)=103.7$, $P<0.001$] and propofol by peptide interaction [$F(1,56)=149$, $P<0.001$]. By *post hoc* analysis, we found decreased synapse number in propofol/TAT-MUT [$n=15$, 0.16 (0.01)] treated animals compared with IL/TAT-MUT [$n=15$, 0.36 (0.01), $P<0.001$] and propofol/TAT-C3 [$n=15$, (0.33 (0.01), $P<0.001$]. Higher magnification (15 000×) images (representative of the four exposure groups shown in Fig. 4m) showed that propofol (after pre-treated with TAT-MUT) reduced the total number of presynaptic vesicles; TAT-C3 pre-treatment reversed the propofol-mediated reductions in total synapse and presynaptic vesicle numbers (Fig. 4m and n). There was a significant effect of propofol treatment [$F(1,56)=34.96$, $P<0.001$], peptide treatment [$F(1,56)=88.98$, $P<0.001$] and propofol by peptide interaction [$F(1,56)=63.6$, $P<0.001$] and there was a reduction in vesicle number by propofol/TAT-MUT [$n=15$, 146 (10)] treated animals compared with IL/TAT-MUT [$n=15$, 278 (9), $P<0.001$] and propofol/TAT-C3 [$n=15$, 311 (9), $P<0.001$].

Propofol exposure of PND 5–7 mouse pups impairs hippocampus-dependent contextual fear memory 3 months after exposure

Propofol exposure of neonatal mice altered hippocampal architecture *in vivo* (Figs 3 and 4): decreased IMF bundle area

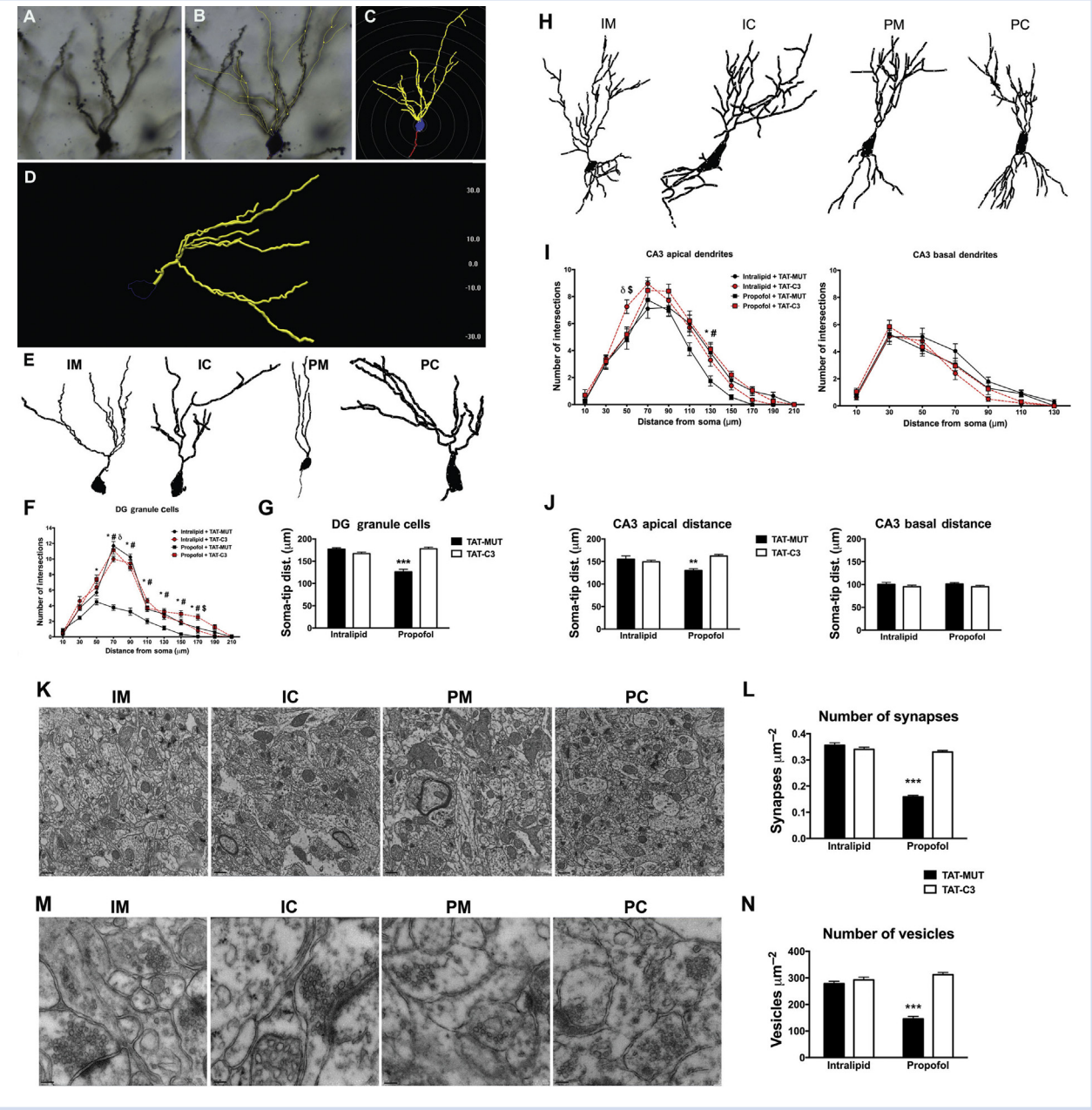

Fig 4. RhoA inhibition with TAT-C3 prevents propofol-mediated reduction in dendritic arborisation, hippocampal synapses, and presynaptic vesicles 4 weeks after exposure. Postnatal day 5–7 mice were pre-treated with TAT-MUT or TAT-C3 (12.5 mg kg^{-1} i.p. 2 h) and then exposed to propofol (50 mg kg^{-1}, 25 mg kg^{-1}, and 25 mg kg^{-1} i.p. injections separated by 2 h) or Intralipid (vehicle control). Four weeks after propofol exposure, hippocampal dendritic arborisation and synapse quantitation were evaluated using Golgi–Cox staining and electron microscopy, respectively. (a) Representative Golgi–Cox stain of granule cell neurones in the DG. (b) Neurones were traced using Neurolucida software. (c) Three-dimensional reconstruction and Sholl analysis. (d) Neuronal tracing with XYZ orientation and corresponding depth measurements (um). (e) Propofol plus TAT-Mut (PM) decreased apical dendritic arborisation and distance from soma in granule cell neurones, an effect prevented with TAT-C3 (PC). (f) Quantitation granule cell apical dendritic arborisation (n=20; ***P<0.001) and (g) dendritic distance from soma (n=20; ***P<0.001). (h) Propofol (PM) decreased CA3 pyramidal cell apical dendritic arborisation and distance from soma, an effect prevented with TAT-C3 (PC); no observed effect occurred on CA3 basal dendrites with propofol. (i) Quantitation of CA3 pyramidal cell apical dendritic arborisation (n=20; **P<0.01) and (j) dendritic distance from soma data (n=20; P=0.76). (k) Electron microscopy of hippocampal synapses (2500× magnification). Propofol (PM) decreased total number of hippocampal synapses; TAT-C3 (PC) prevented propofol-mediated decrease in synapses. (l) Quantitation of synapses (n=15; ***P<0.001) and (n) number of presynaptic vesicles. (m) Representative image (15 000× magnification) of presynaptic vesicles. DG, dentate gyrus; IC, Intralipid/TAT-C3; IM, Intralipid/TAT-mutant; i.p., intraperitoneal; PC, propofol/TAT-C3; PM, propofol/TAT-mutant. Data are presented as mean (SEM). P was assumed significant when $\alpha < 0.05$; *P<0.05, **P<0.01, ***P<0.001; *Propofol + TAT-MUT *vs* Propofol +TAT-C3, $^{\#}$Propofol +TAT-MUT *vs* Intralipid + TAT-MUT, $^{\$}$Propofol + TAT-C3 *vs* Intralipid + TAT-C3, $^{\delta}$Intralipid + TAT-MUT *vs* Intralipid + TAT-C3.

(Fig. 3); decreased dendritic arborisation (Fig 4a–j); decreased total synapse (Fig. 4k and l) and presynaptic vesicle number (Fig. 4m and n). We therefore tested whether propofol exposure of neonatal mice affected hippocampus-dependent learning and memory at age 3 months. Mice were weighed and baseline tested for gross motor function and anxiety in the open field paradigm to exclude any obvious dysfunction before testing learning and memory behaviours (Supplementary Fig. S1). We exposed PND 5–7 mice to propofol or Intralipid (vehicle control) i.p. injection and then assessed cognitive behaviour using a fear conditioning learning and memory test at 3 months of age. Data during the learning phase on day 1 were analysed with a three-way ANOVA (Fig. 5a). We found a significant effect of time [χ^2=33.0, P<0.001, (ε=0.81), F(2.42,120.88)=161.01, P<0.001], with no significant effect of time × propofol [F(2.42,120.88)=1.45, P=0.24], time × peptide [F(2.42,120.88)=2.65, P=0.06], and time × propofol × peptide [F(2.42,120.88)=2.15, P=0.11] for within subjects effects. Group effect revealed effects of the factor peptide [F(1,50)=11.62, P=0.001] and the propofol × peptide interaction [F(1,50)=9.62, P=0.003] with lower freezing to the tone presentation during the learning phase for propofol/TAT-MUT treated mice compared with IL/TAT-MUT (tone 2, P<0.05) and propofol/TAT-C3 (tone 2 and tone 3, P<0.01). On day 2, animals were re-exposed to context and analysis showed a significant effect of propofol × peptide interaction [F(1,50)=8.76, P=0.005] with decreased freezing in propofol/MUT animals [n=14, 30 (3)] compared with IL/TAT-MUT [n=10, 43 (4)]. On day 3, mice were re-exposed to the cue and showed a significant effect for the factor propofol [F(1,50)=4.28, P=0.04] and no significant comparisons between groups. *Post hoc* power analysis for ANOVA with an effect size f=0.4, α=0.05, yielded a total sample size of n=54 degrees of freedom (dfn)=1 and four groups as a representative for our fear conditioning analysis (Fig. 5b and c). The results yielded a critical F value of 4.03 and 1−β=0.82. Based on this, with an effect size of 0.4 and our current group size, our study has a statistical power of 82%. These data indicate that propofol/TAT-MUT treated mice had deficits during cued learning (day 1) and context recollection (day 2), a deficit that was prevented by TAT-C3 pre-treatment, while an overall effect of propofol was observed during cue presentation on day 3 (Fig. 5a–c).

Discussion

Propofol exposure of neonatal neurons, both *in vitro* and *in vivo*, results in growth cone collapse, impairment in axonal transport of key neurotrophin positive vesicles, retraction of hippocampal mossy fibre networks, altered hippocampal dendritic arborisation, and decreases in total synapse and presynaptic vesicle number, all of which were accompanied by cognitive deficits. These neuropathological changes were prevented by TAT-C3, a small peptide that inhibits RhoA activation, suggesting that RhoA activation plays a critical role in propofol-mediated neurotoxicity. This is the first study to show that neonatal propofol-induced neurotoxicity is associated, at least in part, with changes in axonal transport of neurotrophic factors (BDNF) and altered neuronal connectivity.

Studies of anaesthetic-mediated neurotoxicity in neonates has focused largely on apoptosis.[1–4,6,8–17,73–75] While it is logical to surmise that neuronal loss during development should result in cognitive deficits, there have been animal studies challenging this notion.[5,18,19] Anaesthetic exposure in neonates can induce cognitive dysfunction without neuronal apoptosis, and apoptosis can occur without resultant impairments in learning and memory.[5,18,20] In fact, hypercarbia-induced apoptosis in neonatal rodents actually improves cognitive function later in life.[18] While there is no doubt that anaesthesia induces neuroapoptosis beyond normal development, there is the possibility that other mechanisms contribute to the observed cognitive deficits with early anaesthetic exposure.

Synaptogenesis and neuronal circuit formation during development determines later cognitive function.[54,57,58,66] Formation of neuronal networks requires appropriate dendritic and axonal form/function.[23,25,48–50,65,76] Either isoflurane or propofol exposure of neonatal neurones results in dendritic

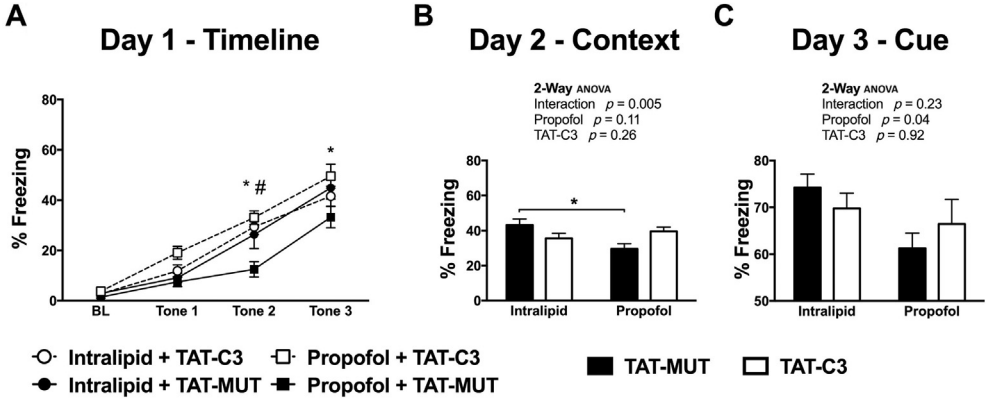

Fig 5. Propofol exposure of neonatal mouse pups impairs hippocampus-dependent contextual fear memory in mice 3 months after exposure. Fear conditioning was used to assess learning and memory 3 months after propofol exposure. Postnatal day 5–7 mice received i.p. injections of propofol or Intralipid (control) and assessed for cognitive behaviour at age 3 months. Mice that received propofol plus TAT-MUT exhibited deficits in (a) cued learning (day 1) and (b) context re-exposure (day 2), a deficit that was prevented with TAT-C3. (c) No effect was observed on cued re-exposure on day 3. n=10–16 per group; data presented as mean (SEM); P was assumed significant when α < 0.05; *P<0.05, **P<0.01, ***P<0.001; *Propofol + TAT-MUT *vs* Propofol +TAT-C3, #Propofol +TAT-MUT *vs* Intralipid + TAT-MUT. ANOVA, analysis of variance; i.p., intraperitoneal.

spine loss; these changes are ameliorated by RhoA kinase inhibition, suggesting a role for RhoA activation and actin dysregulation.[11–13,23,77] The effects of anaesthetics on dendritic ultrastructure have been well characterised; however, little is known about anaesthetic effects on axonal components of synaptic and neuronal network formation, such as growth cone morphology and axonal transport. The *in vitro* findings herein address how propofol can alter axonal components of development. We show that propofol induces growth cone collapse and impairs axonal transport of BDNF, both of which influence neurone motility, target pathfinding, and synaptic strength and maintenance.[23,50,78] Propofol-induced growth cone collapse and axonal transport deficits were prevented with RhoA inhibitor pre-treatment, suggesting RhoA is critical for propofol-mediated alterations in dendritic and axonal development. Our findings are consistent with other data showing RhoGTPase (RhoA, Rac1, and Cdc42) signalling regulation and balance is essential for growth cone morphology and function, axonal transport, and neuronal extension during development.[23,27,32,33,50,79–81]

While our *in vitro* findings provide new insights into the mechanism(s) for propofol-mediated neurotoxicity, we are still in the preliminary stages of better understanding how propofol and other anaesthetics activate RhoA to alter neuronal development. It is unclear whether propofol alters other Rho GTPases, such as Rac1 and Cdc42. Anaesthetised, electrically 'silenced', or both neurones exhibit increased proBDNF signalling relative to mature BDNF (mBDNF) signalling.[11–13,82] ProBDNF binds to the $p75^{NTR}$ receptor to activate RhoA,[83,84] while mBDNF binds to the TrkB receptor to activate Rac1/Cdc42.[85,86] It is conceivable that propofol-induced $p75^{NTR}$,signalling leads to increased RhoA activation with a concomitant decrease in mBDNF activation of TrkB and Rac1/Cdc42 signalling, altering the 'yin and yang' of Rho GTPase signalling that is pivotal during development.[11–13,23,86,87] Therefore, protecting neurones against anaesthetic-mediated neurotoxicity, by balancing overall Rho GTPase signalling, might be achieved through either RhoA inhibition (as seen herein) or Rac1/Cdc42 activation.[23,88]

The importance of properly balanced Rho GTPase activity to protect against anaesthetic-mediated neurotoxicity is revealed in a previous study from our group showing that the use of TAT-Pep5 before isoflurane exposure did not prevent cognitive dysfunction.[21] TAT-Pep5 inhibits RhoA activation by preventing $p75^{NTR}$-induced displacement of RhoA from RhoGDIs (Rho GDP-dissociation inhibitors); this results in a small pool of RhoA that cannot be activated.[89] That TAT-Pep5 only prevents activation of a small fraction of the total RhoA may explain why it does not prevent isoflurane-induced cognitive dysfunction in our previous study.[21] By contrast, TAT-C3 inhibits RhoA activation through ADP ribosylation of RhoA-GDP; this mechanism targets a larger fraction of RhoA, which may account for its ability to prevent propofol-mediated cognitive deficits.

A challenge in better understanding how propofol alters Rho GTPase activity is the promiscuity between RhoA, Rac1, and Cdc42 and the multiple upstream receptors; signalling is not limited to TrkB and $p75^{NTR}$. Other receptors that influence Rho GTPases include plexin, glutamate, $GABA_A$, notch, and integrins.[90] There are many intermediary molecules that influence Rho GTPase activation; these include DISC1 and Cdk5.[90] After Rho GTPases are activated, the effects on actin dynamics are executed through many effector proteins, including cofilin, CRMP-2, and myosin-II.[23,25] Collectively, the number of receptors that converge upon Rho GTPase signalling, along with the diversity of downstream effector proteins that regulate actin dynamics, makes Rho GTPase signalling complex. While there are still gaps in knowledge, our results are an initial and important step in better understanding of how propofol alters Rho GTPase signalling and influences neuronal development. Collectively, our findings advance our understanding of propofol-mediated neurotoxicity, describe a novel mechanism, set the stage for further investigations, and identify potential therapeutic targets.

The observation that propofol alters retrograde axonal transport of BDNF is particularly noteworthy as we are the first to describe this pathological phenotype in neurones exposed to propofol. Deficits in retrograde axonal transport of trophic factor have been linked to cognitive impairment in many disorders such as Down's syndrome, Alzheimer's disease, and Huntington's disease.[78,91–97] The causes of axonal transport deficits in these neurological disorders are multifaceted, affecting several components of the axonal transport machinery.[30,78,96,98–102] Normal retrograde axonal transport of neurotrophins requires binding to surface receptors (i.e. TrkA, TrkB), endocytosis, recruitment of effector proteins and motor proteins, and access to axonal microtubules for guided transport.[30,44,102–104] Amongst the recruited signalling endosome effector proteins are Rho GTPases (RhoA, Rac1/Cdc42).[30,102] Rho GTPase and actin regulation are important for competent retrograde axonal transport.[30,102] Given that propofol activates RhoA to alter actin regulation, it is not surprising that there is impaired transport of BDNF, and that these impairments are improved with RhoA inhibition and balanced Rho GTPase signalling; these findings are consistent with previous work.[11–13,30,102]

Previously, we have shown that isoflurane induces neurotoxicity by preventing conversion of proBDNF to mBDNF, which results in preferential $p75^{NTR}$ signalling.[11] Increased $p75^{NTR}$ signalling leads to increased RhoA activation and actin dysregulation, and actin dysregulation at the growth cone impairs retrograde axonal transport of neurotrophins.[30] Our findings are a logical extension of our previous findings that propofol causes increased proBDNF induced $p75^{NTR}$ signalling, RhoA activation, actin dysregulation, and impaired axonal transport of neurotrophins. While we investigated the transport of exogenous QD-BDNF, it is likely that endogenous mBDNF transport is impaired as well based on the suggestion that the transport defect is at the level of endocytosis and signalling endosome formation, factors influenced by actin dynamics.[30] A more thorough investigation is needed to better understand how propofol impairs endocytosis and formation of signalling endosome. The impact of propofol on other axonal transport components (i.e. motor proteins and microtubules), if any, will also be addressed in future studies.

Our *in vitro* findings that propofol causes RhoA-dependent loss of dendritic spines, growth cone collapse, and impaired retrograde axonal transport of BDNF led to experiments to determine if similar effects occur *in vivo*. Our data suggest that both dendritic and axonal components of neuronal development in the hippocampus are negatively impacted by neonatal exposure to propofol, and that these changes are associated with impaired learning and memory. Moreover, propofol-associated developmental defects *in vivo* are also caused by RhoA activation as evidenced by the observation that administration of a RhoA inhibitor before propofol exposure prevented neurotoxicity.

Learning and memory are largely dependent on neuronal networks within the hippocampus.[57,105–107] A region of particular importance is the IMF bundle, which arises from axons of dentate gyrus granule cells and synapse onto CA3 neurone apical dendrites.[55,57,108] Formation and pruning of the infrapyramidal bundle during development is important for later cognition.[53,66,109] Axonal pathfinding from the dentate gyrus to the CA3 region requires properly coordinated growth cone motility, along with normal retrograde axonal transport of neurotrophins.[23,25,45–47,58,62] Given that propofol causes growth cone collapse and impaired retrograde axonal transport *in vitro*, it is mechanistically consistent that infrapyramidal bundle area is decreased 28 days after propofol exposure. Additionally, infrapyramidal synapses with CA3 apical dendrites provide trophic support and encourage dendritic arborisation.[65,110] As such, loss of infrapyramidal innervation to the CA3 region might contribute to reduced CA3 apical dendrite length and branching in mice exposed to propofol. Evidence that propofol decreases infrapyramidal axonal projections and impairs apical dendritic arborisation was supported by our findings that mice exposed to propofol exhibited loss of hippocampal synapses and presynaptic vesicles. Taken together, we believe that propofol-induced RhoA activation causes an imbalance in actin dynamics, resulting in altered infrapyramidal pathfinding to the CA3 region, blunted trophic support, decreased dendritic arborisation, and deficits in learning and memory. It is still unclear if defective infrapyramidal pathfinding is the only mechanism for decreased hippocampal synapse number and dendritic arborisation. It is possible that increased RhoA activation also acts directly at dendrites to cause dysregulation of actin and loss of dendritic arborisation that are related to synaptic activity and contribute to learning and memory.[111,112]

Further investigation is needed to better understand why other anaesthetics, such as ketamine, affect the infrapyramidal bundle differently than propofol; for example, ketamine exposure of neonatal rodents results in decreased infrapyramidal pruning.[113] Propofol acts primarily through γ-aminobutyric acid agonism, while ketamine acts through N-methyl-D-aspartate receptor antagonism. There is evidence for a complex interplay between dimethylnitrosamine receptor activity and Rho GTPase activation.[114,115] It is plausible that ketamine alters Rho GTPase signalling to favour actin polymerisation, leading to decreased pruning. Propofol leads to actin collapse, which might account for the loss of infrapyramidal bundles observed. These differences between propofol and ketamine need to be explored in future studies. It is likely that altered pruning (either too much or too little) alters synaptic connections that results in cognitive deficits.

Despite the logical mechanistic connection between our *in vitro*, *in vivo*, and behavioural data, there remains the concern that neurones might mature and behave differently in a culture dish compared with their *in vivo* environment. There are few published data that compare how neurones mature *in vitro* and *in vivo* in the current toxicity model. However, other studies have used developing neurones of similar *in vitro* and *in vivo* age to show that the mechanisms for hippocampal development are similar in both environments.[116] Despite the confidence that our *in vitro* and *in vivo* findings are mechanistically linked, future studies will aim to confirm that exposing neonatal mice to propofol causes growth cone collapse and impairs axonal transport of neurotrophins *in vivo*.

In conclusion, our findings show that propofol exposure of neonatal neurones results in RhoA activation, growth cone collapse, impaired axonal transport of BDNF, altered hippocampal circuitry, and cognitive deficits. We are the first to propose altered neuronal pathfinding and connectivity as a mechanism for propofol-mediated neurotoxicity. Future research will address the following questions: (1) is the neurotoxicity seen with other anaesthetic; (2) are other Rho GTPases affected; (3) what are the contributing upstream and downstream signalling pathways from RhoA; and (4) are other components of axonal transport impaired? These studies could identify important therapeutic targets should anaesthetic-mediated neurotoxicity prove relevant in humans.

Authors' contributions

Study design: M.P., B.H.
Acquisition of *in vitro* data: M.P., M.K., B.H.
Analysis of *in vitro* data: M.P., B.H.
Interpretation of all data: M.P., H.H.P., P.M., B.H.
Writing up of the first draft of the manuscript: M.P., B.H.
Manuscript editing: M.P., J.S., C.W., C.M., J.B., C.D., B.L., R.H., W.M., H.H.P., P.M., B.H.
Acquisition of behavioural data: J.S.
Analysis of behavioural data: J.S.
Statistical analysis of all data: J.S.
Interpretation of behavioural data: J.S.
Intraperitoneal delivery of propofol to mouse pups: M.J., J.E.
Immunofluorescence data acquisition and analysis: M.J., J.E.
Electron microscopy data acquisition and analysis: M.J., J.E., S.M.
Golgi–Cox staining and analysis: M.J.
Study design of *in vitro* axonal transport experiments: C.W.
Interpretation of *in vitro* data: C.W.
Staining, imaging, analysis and interpretation of Golgi–Cox data: C.M., M.F., U.N.
Expert consultation for all TAT-C3 experiments: J.B.
Assistance with *in vitro* study design: W.M.
Assistance with study design: H.H.P., P.M.
Golgi-Cox staining and analysis: C.M.
EM data analysis: B.H.

Declarations of interest

The authors declare no conflicting financial interest.

Funding

Work in the authors' laboratories is supported by Mentored Research Training Grant-BS from the Foundation for Anesthesia Education and Research (MLP), Veteran Affairs Merit Award from the Department of Veterans Affairs BX003671 (BPH) and BX001963 (HHP), National Institutes of Health, Bethesda, MD, USA, NS073653 (BPH); HL091071 and HL107200 (HHP); GM085179 (PMP); DA034140 and AA020098 (CDM).

Appendix A. Supplementary data

Supplementary data related to this article can be found at https://doi.org/10.1016/j.bja.2017.12.033.

References

1. Boscolo A, Milanovic D, Starr JA, et al. Early exposure to general anesthesia disturbs mitochondrial fission and fusion in the developing rat brain. *Anesthesiology* 2013; **118**: 1086–97

2. Boscolo A, Ori C, Bennett J, Wiltgen B, Jevtovic-Todorovic V. Mitochondrial protectant pramipexole prevents sex-specific long-term cognitive impairment from early anaesthesia exposure in rats. *Br J Anaesth* 2013; **110**: i47–52
3. Jevtovic-Todorovic V, Beals J, Benshoff N, Olney JW. Prolonged exposure to inhalational anesthetic nitrous oxide kills neurons in adult rat brain. *Neuroscience* 2003; **122**: 609–16
4. Popic J, Pesic V, Milanovic D, et al. Propofol-induced changes in neurotrophic signaling in the developing nervous system in vivo. *PLoS One* 2012; **7**, e34396
5. Fredriksson A, Pontén E, Gordh T, Eriksson P. Neonatal exposure to a combination of N-methyl-D-aspartate and gamma-aminobutyric acid type A receptor anesthetic agents potentiates apoptotic neurodegeneration and persistent behavioral deficits. *Anesthesiology* 2007; **107**: 427–36
6. Soriano SG, Liu Q, Li J, et al. Ketamine activates cell cycle signaling and apoptosis in the neonatal rat brain. *Anesthesiology* 2010; **112**: 1155–63
7. Briner A, Nikonenko I, De Roo M, Dayer A, Muller D, Vutskits L. Developmental stage-dependent persistent impact of propofol anesthesia on dendritic spines in the rat medial prefrontal cortex. *Anesthesiology* 2011; **115**: 282–93
8. Boscolo A, Starr JA, Sanchez V, et al. The abolishment of anesthesia-induced cognitive impairment by timely protection of mitochondria in the developing rat brain: the importance of free oxygen radicals and mitochondrial integrity. *Neurobiol Dis* 2012; **45**: 1031–41
9. Jevtovic-Todorovic V, Boscolo A, Sanchez V, Lunardi N. Anesthesia-induced developmental neurodegeneration: the role of neuronal organelles. *Front Neurol* 2012; **3**: 141
10. Lu LX, Yon JH, Carter LB, Jevtovic-Todorovic V. General anesthesia activates BDNF-dependent neuroapoptosis in the developing rat brain. *Apoptosis* 2006; **11**: 1603–15
11. Head BP, Patel HH, Niesman IR, Drummond JC, Roth DM, Patel PM. Inhibition of p75 neurotrophin receptor attenuates isoflurane-mediated neuronal apoptosis in the neonatal central nervous system. *Anesthesiology* 2009; **110**: 813–25
12. Lemkuil BP, Head BP, Pearn ML, Patel HH, Drummond JC, Patel PM. Isoflurane neurotoxicity is mediated by p75NTR-RhoA activation and actin depolymerization. *Anesthesiology* 2011; **114**: 49–57
13. Pearn ML, Hu Y, Niesman IR, et al. Propofol neurotoxicity is mediated by p75 neurotrophin receptor activation. *Anesthesiology* 2012; **116**: 352–61
14. Cattano D, Young C, Straiko MM, Olney JW. Subanesthetic doses of propofol induce neuroapoptosis in the infant mouse brain. *Anesth Analg* 2008; **106**: 1712–4
15. Jevtovic-Todorovic V, Hartman RE, Izumi Y, et al. Early exposure to common anesthetic agents causes widespread neurodegeneration in the developing rat brain and persistent learning deficits. *J Neurosci* 2003; **23**: 876–82
16. Johnson SA, Young C, Olney JW. Isoflurane-induced neuroapoptosis in the developing brain of nonhypoglycemic mice. *J Neurosurg Anesthesiol* 2008; **20**: 21–8
17. Olney JW, Wozniak DF, Jevtovic-Todorovic V, Farber NB, Bittigau P, Ikonomidou C. Drug-induced apoptotic neurodegeneration in the developing brain. *Brain Pathol* 2002; **12**: 488–98
18. Stratmann G, May LD, Sall JW, et al. Effect of hypercarbia and isoflurane on brain cell death and neurocognitive dysfunction in 7-day-old rats. *Anesthesiology* 2009; **110**: 849–61
19. Loepke AW, Istaphanous GK, McAuliffe 3rd JJ, et al. The effects of neonatal isoflurane exposure in mice on brain cell viability, adult behavior, learning, and memory. *Anesth Analg* 2009; **108**: 90–104
20. Lee BH, Chan JT, Hazarika O, Vutskits L, Sall JW. Early exposure to volatile anesthetic impairs long-term associative learning and recognition memory. *PLoS One* 2014; **9**, e105340
21. Schilling JM, Kassan A, Mandyam C, et al. Inhibition of p75 neurotrophin receptor does not rescue cognitive impairment in adulthood after isoflurane exposure in neonatal mice. *Br J Anaesth* 2017; **119**: 465–71
22. Cosker KE, Segal RA. Neuronal signaling through endocytosis. *Cold Spring Harb Perspect Biol* 2014; **6**. a020669
23. Hall A, Lalli G. Rho and Ras GTPases in axon growth, guidance, and branching. *Cold Spring Harb Perspect Biol* 2010; **2**. a001818
24. Stokin GB, Goldstein LS. Axonal transport and Alzheimer's disease. *Annu Rev Biochem* 2006; **75**: 607–27
25. Dent EW, Gupton SL, Gertler FB. The growth cone cytoskeleton in axon outgrowth and guidance. *Cold Spring Harb Perspect Biol* 2011; **3**. a001800
26. Gallo G. RhoA-kinase coordinates F-actin organization and myosin II activity during semaphorin-3A-induced axon retraction. *J Cell Sci* 2006; **119**: 3413–23
27. Kozma R, Sarner S, Ahmed S, Lim L. Rho family GTPases and neuronal growth cone remodelling: relationship between increased complexity induced by Cdc42Hs, Rac1, and acetylcholine and collapse induced by RhoA and lysophosphatidic acid. *Mol Cell Biol* 1997; **17**: 1201–11
28. Wu KY, Hengst U, Cox LJ, et al. Local translation of RhoA regulates growth cone collapse. *Nature* 2005; **436**: 1020–4
29. Goshima Y, Hida T, Gotoh T. Computational analysis of axonal transport: a novel assessment of neurotoxicity, neuronal development and functions. *Int J Mol Sci* 2012; **13**: 3414–30
30. Harrington AW, St Hillaire C, Zweifel LS, et al. Recruitment of actin modifiers to TrkA endosomes governs retrograde NGF signaling and survival. *Cell* 2011; **146**: 421–34
31. Amano M, Nakayama M, Kaibuchi K. Rho-kinase/ROCK: a key regulator of the cytoskeleton and cell polarity. *Cytoskeleton* 2010; **67**: 545–54
32. Ng J, Luo L. Rho GTPases regulate axon growth through convergent and divergent signaling pathways. *Neuron* 2004; **44**: 779–93
33. Govek EE, Hatten ME, Van Aelst L. The role of Rho GTPase proteins in CNS neuronal migration. *Dev Neurobiol* 2011; **71**: 528–53
34. Wittmann T, Waterman-Storer CM. Cell motility: can Rho GTPases and microtubules point the way? *J Cell Sci* 2001; **114**: 3795–803
35. Zhao X, Zhou Y, Weissmiller AM, Pearn ML, Mobley WC, Wu C. Real-time imaging of axonal transport of quantum dot-labeled BDNF in primary neurons. *J Vis Exp* 2014; **91**: 51899
36. Sung K, Maloney MT, Yang J, Wu C. A novel method for producing mono-biotinylated, biologically active neurotrophic factors: an essential reagent for single molecule

study of axonal transport. *J Neurosci Meth* 2011; **200**: 121–8
37. Head BP, Patel HH, Roth DM, et al. G-protein-coupled receptor signaling components localize in both sarcolemmal and intracellular caveolin-3-associated microdomains in adult cardiac myocytes. *J Biol Chem* 2005; **280**: 31036–44
38. Egawa J, Zemljic-Harpf AE, Mandyam CD, et al. Neuron-targeted caveolin-1 promotes ultrastructural and functional hippocampal synaptic plasticity. *Cereb Cortex* July 31, 2017: 1–12. https://doi.org/10.1093/cercor/bhx196. Advance Access published on
39. Mandyam CD, Schilling JM, Cui W, et al. Neuron-targeted caveolin-1 improves molecular signaling, plasticity, and behavior dependent on the hippocampus in adult and aged mice. *Biol Psychiatry* 2017; **81**: 101–10
40. Sebbagh M, Renvoize C, Hamelin J, Riche N, Bertoglio J, Breard J. Caspase-3-mediated cleavage of ROCK I induces MLC phosphorylation and apoptotic membrane blebbing. *Nat Cell Biol* 2001; **3**: 346–52
41. Sahai E, Olson MF. Purification of TAT-C3 exoenzyme. *Methods Enzymol* 2006; **406**: 128–40
42. Ribeiro A, Balasubramanian S, Hughes D, Vargo S, Powell EM, Leach JB. beta1-Integrin cytoskeletal signaling regulates sensory neurons response to matrix dimensionality. *Neuroscience* 2013; **248**: 67–78
43. Tsushima H, Emanuele M, Polenghi A, et al. HDAC6 and RhoA are novel players in Abeta-driven disruption of neuronal polarity. *Nat Commun* 2015; **6**: 7781
44. Bartlett SE, Reynolds AJ, Hendry IA. Retrograde axonal transport of neurotrophins: differences between neuronal populations and implications for motor neuron disease. *Immunol Cell Biol* 1998; **76**: 419–23
45. Kobayashi K. Hippocampal mossy fiber synaptic transmission and its modulation. *Vitam Horm* 2010; **82**: 65–85
46. Koyama R, Yamada MK, Nishiyama N, Matsuki N, Ikegaya Y. Developmental switch in axon guidance modes of hippocampal mossy fibers in vitro. *Dev Biol* 2004; **267**: 29–42
47. Faux CH, Parnavelas JG. The role of intracellular calcium and RhoA in neuronal migration. *Sci STKE* 2007; **2007**. pe62
48. Kalil K, Szebenyi G, Dent EW. Common mechanisms underlying growth cone guidance and axon branching. *J Neurobiol* 2000; **44**: 145–58
49. Kalil K, Dent EW. Touch and go: guidance cues signal to the growth cone cytoskeleton. *Curr Opin Neurobiol* 2005; **15**: 521–6
50. Mulherkar S, Liu F, Chen Q, et al. The small GTPase RhoA is required for proper locomotor circuit assembly. *PLoS One* 2013; **8**, e67015
51. Santos Da Silva J, Schubert V, Dotti CG. RhoA, Rac1, and cdc42 intracellular distribution shift during hippocampal neuron development. *Mol Cell Neurosci* 2004; **27**: 1–7
52. Winding M, Kelliher MT, Lu W, Wildonger J, Gelfand VI. Role of kinesin-1-based microtubule sliding in Drosophila nervous system development. *Proc Natl Acad Sci U S A* 2016; **113**: E4985–94
53. Crusio WE, Schwegler H. Early postnatal hyperthyroidism improves both working and reference memory in a spatial radial-maze task in adult mice. *Physiol Behav* 1991; **50**: 259–61
54. Crusio WE, Schwegler H. Learning spatial orientation tasks in the radial-maze and structural variation in the hippocampus in inbred mice. *Behav Brain Funct* 2005; **1**: 3
55. Romer B, Krebs J, Overall RW, et al. Adult hippocampal neurogenesis and plasticity in the infrapyramidal bundle of the mossy fiber projection: I. Co-regulation by activity. *Front Neurosci* 2011; **5**: 107
56. Prince LY, Bacon TJ, Tigaret CM, Mellor JR. Neuromodulation of the feedforward dentate gyrus-CA3 Microcircuit. *Front Synaptic Neurosci* 2016; **8**: 32
57. Ramirez-Amaya V, Balderas I, Sandoval J, Escobar ML, Bermudez-Rattoni F. Spatial long-term memory is related to mossy fiber synaptogenesis. *J Neurosci* 2001; **21**: 7340–8
58. Isgor C, Pare C, McDole B, Coombs P, Guthrie K. Expansion of the dentate mossy fiber-CA3 projection in the brain-derived neurotrophic factor-enriched mouse hippocampus. *Neuroscience* 2015; **288**: 10–23
59. Nakayama AY, Luo L. Intracellular signaling pathways that regulate dendritic spine morphogenesis. *Hippocampus* 2000; **10**: 582–6
60. Nakayama AY, Harms MB, Luo L. Small GTPases Rac and Rho in the maintenance of dendritic spines and branches in hippocampal pyramidal neurons. *J Neurosci* 2000; **20**: 5329–38
61. Tashiro A, Minden A, Yuste R. Regulation of dendritic spine morphology by the rho family of small GTPases: antagonistic roles of Rac and Rho. *Cereb Cortex* 2000; **10**: 927–38
62. Koyama R, Ikegaya Y. Mossy fiber sprouting as a potential therapeutic target for epilepsy. *Curr Neurovasc Res* 2004; **1**: 3–10
63. Goodman LA, Model PG. Superinnervation enhances the dendritic branching pattern of the Mauthner cell in the developing axolotl. *J Neurosci* 1988; **8**: 776–91
64. Kossel AH, Williams CV, Schweizer M, Kater SB. Afferent innervation influences the development of dendritic branches and spines via both activity-dependent and non-activity-dependent mechanisms. *J Neurosci* 1997; **17**: 6314–24
65. Riccomagno MM, Kolodkin AL. Sculpting neural circuits by axon and dendrite pruning. *Annu Rev Cell Dev Biol* 2015; **31**: 779–805
66. Kvajo M, McKellar H, Drew LJ, et al. Altered axonal targeting and short-term plasticity in the hippocampus of Disc1 mutant mice. *Proc Natl Acad Sci U S A* 2011; **108**: E1349–58
67. Rohrbeck A, Just I. Cell entry of C3 exoenzyme from Clostridium botulinum. *Curr Top Microbiol Immunol* 2017; **406**: 97–118
68. Redmond L, Ghosh A. The role of Notch and Rho GTPase signaling in the control of dendritic development. *Curr Opin Neurobiol* 2001; **11**: 111–7
69. Zhu YB, Kang K, Zhang Y, et al. PLD1 negatively regulates dendritic branching. *J Neurosci* 2012; **32**: 7960–9
70. Couch BA, DeMarco GJ, Gourley SL, Koleske AJ. Increased dendrite branching in AbetaPP/PS1 mice and elongation of dendrite arbors by fasudil administration. *J Alzheimers Dis* 2010; **20**: 1003–8
71. Ba W, Nadif Kasri N. RhoGTPases at the synapse: an embarrassment of choice. *Small GTPases* 2016: 1–8
72. Ba W, Yan Y, Reijnders MR, et al. TRIO loss of function is associated with mild intellectual disability and affects dendritic branching and synapse function. *Hum Mol Genet* 2016; **25**: 892–902
73. Brambrink AM, Evers AS, Avidan MS, et al. Isoflurane-induced neuroapoptosis in the neonatal rhesus macaque brain. *Anesthesiology* 2010; **112**: 834–41

74. Zou X, Patterson TA, Sadovova N, et al. Potential neurotoxicity of ketamine in the developing rat brain. *Toxicol Sci* 2009; **108**: 149–58
75. Zou X, Patterson TA, Divine RL, et al. Prolonged exposure to ketamine increases neurodegeneration in the developing monkey brain. *Int J Dev Neurosci* 2009; **27**: 727–31
76. Dent EW, Merriam EB, Hu X. The dynamic cytoskeleton: backbone of dendritic spine plasticity. *Curr Opin Neurobiol* 2011; **21**: 175–81
77. Vutskits L, Gascon E, Tassonyi E, Kiss JZ. Clinically relevant concentrations of propofol but not midazolam alter in vitro dendritic development of isolated gamma-aminobutyric acid-positive interneurons. *Anesthesiology* 2005; **102**: 970–6
78. Chevalier-Larsen E, Holzbaur EL. Axonal transport and neurodegenerative disease. *Biochim Biophys Acta* 2006; **1762**: 1094–108
79. Arpaia E, Blaser H, Quintela-Fandino M, et al. The interaction between caveolin-1 and Rho-GTPases promotes metastasis by controlling the expression of alpha5-integrin and the activation of Src, Ras and Erk. *Oncogene* 2012; **31**: 884–96
80. Grande-Garcia A, Echarri A, de Rooij J, et al. Caveolin-1 regulates cell polarization and directional migration through Src kinase and Rho GTPases. *J Cell Biol* 2007; **177**: 683–94
81. Joshi B, Strugnell SS, Goetz JG, et al. Phosphorylated caveolin-1 regulates Rho/ROCK-dependent focal adhesion dynamics and tumor cell migration and invasion. *Cancer Res* 2008; **68**: 8210–20
82. Je HS, Yang F, Ji Y, Nagappan G, Hempstead BL, Lu B. Role of pro-brain-derived neurotrophic factor (proBDNF) to mature BDNF conversion in activity-dependent competition at developing neuromuscular synapses. *Proc Natl Acad Sci U S A* 2012; **109**: 15924–9
83. Sun Y, Lim Y, Li F, et al. ProBDNF collapses neurite outgrowth of primary neurones by activating RhoA. *PLoS One* 2012; **7**, e35883
84. Riffault B, Medina I, Dumon C, et al. Pro-brain-derived neurotrophic factor inhibits GABAergic neurotransmission by activating endocytosis and repression of GABAA receptors. *J Neurosci* 2014; **34**: 13516–34
85. Miyamoto Y, Yamauchi J, Tanoue A, Wu C, Mobley WC. TrkB binds and tyrosine-phosphorylates Tiam1, leading to activation of Rac1 and induction of changes in cellular morphology. *Proc Natl Acad Sci U S A* 2006; **103**: 10444–9
86. Hedrick NG, Harward SC, Hall CE, Murakoshi H, McNamara JO, Yasuda R. Rho GTPase complementation underlies BDNF-dependent homo- and heterosynaptic plasticity. *Nature* 2016; **538**: 104–8
87. Auer M, Hausott B, Klimaschewski L. Rho GTPases as regulators of morphological neuroplasticity. *Ann Anat* 2011; **193**: 259–66
88. Stankiewicz TR, Linseman DA. Rho family GTPases: key players in neuronal development, neuronal survival, and neurodegeneration. *Front Cell Neurosci* 2014; **8**: 314
89. Yamashita T, Tohyama M. The p75 receptor acts as a displacement factor that releases Rho from Rho-GDI. *Nat Neurosci* 2003; **6**: 461–7
90. Vadodaria KC, Jessberger S. Maturation and integration of adult born hippocampal neurons: signal convergence onto small Rho GTPases. *Front Synaptic Neurosci* 2013; **5**: 4
91. Salehi A, Delcroix JD, Belichenko PV, et al. Increased App expression in a mouse model of Down's syndrome disrupts NGF transport and causes cholinergic neuron degeneration. *Neuron* 2006; **51**: 29–42
92. Poon WW, Blurton-Jones M, Tu CH, et al. Beta-amyloid impairs axonal BDNF retrograde trafficking. *Neurobiol Aging* 2011; **32**: 821–33
93. Zhao X, Chen XQ, Han E, et al. TRiC subunits enhance BDNF axonal transport and rescue striatal atrophy in Huntington's disease. *Proc Natl Acad Sci U S A* 2016; **113**: E5655–64
94. Kruttgen A, Saxena S, Evangelopoulos ME, Weis J. Neurotrophins and neurodegenerative diseases: receptors stuck in traffic? *J Neuropathol Exp Neurol* 2003; **62**: 340–50
95. Bronfman FC, Escudero CA, Weis J, Kruttgen A. Endosomal transport of neurotrophins: roles in signaling and neurodegenerative diseases. *Dev Neurobiol* 2007; **67**: 1183–203
96. Millecamps S, Julien JP. Axonal transport deficits and neurodegenerative diseases. *Nat Rev Neurosci* 2013; **14**: 161–76
97. Weissmiller AM, Wu C. Current advances in using neurotrophic factors to treat neurodegenerative disorders. *Transl Neurodegener* 2012; **1**: 14
98. Caviston JP, Holzbaur EL. Microtubule motors at the intersection of trafficking and transport. *Trends Cell Biol* 2006; **16**: 530–7
99. Maday S, Twelvetrees AE, Moughamian AJ, Holzbaur EL. Axonal transport: cargo-specific mechanisms of motility and regulation. *Neuron* 2014; **84**: 292–309
100. Duncan JE, Goldstein LS. The genetics of axonal transport and axonal transport disorders. *PLoS Genet* 2006; **2**: e124
101. Perlson E, Maday S, Fu MM, Moughamian AJ, Holzbaur EL. Retrograde axonal transport: pathways to cell death? *Trends Neurosci* 2010; **33**: 335–44
102. Harrington AW, Ginty DD. Long-distance retrograde neurotrophic factor signalling in neurons. *Nat Rev Neurosci* 2013; **14**: 177–87
103. Chowdary PD, Che DL, Cui B. Neurotrophin signaling via long-distance axonal transport. *Annu Rev Phys Chem* 2012; **63**: 571–94
104. Butowt R, von Bartheld CS. Fates of neurotrophins after retrograde axonal transport: phosphorylation of p75NTR is a sorting signal for delayed degradation. *J Neurosci* 2009; **29**: 10715–29
105. Treves A, Rolls ET. Computational analysis of the role of the hippocampus in memory. *Hippocampus* 1994; **4**: 374–91
106. Burgess N, Maguire EA, O'Keefe J. The human hippocampus and spatial and episodic memory. *Neuron* 2002; **35**: 625–41
107. Smith DM, Mizumori SJ. Hippocampal place cells, context, and episodic memory. *Hippocampus* 2006; **16**: 716–29
108. Krebs J, Romer B, Overall RW, et al. Adult hippocampal neurogenesis and plasticity in the infrapyramidal bundle of the mossy fiber projection: II. Genetic covariation and identification of Nos1 as linking candidate gene. *Front Neurosci* 2011; **5**: 106
109. Faulkner RL, Low LK, Cheng HJ. Axon pruning in the developing vertebrate hippocampus. *Dev Neurosci* 2007; **29**: 6–13
110. Amaral DG, Scharfman HE, Lavenex P. The dentate gyrus: fundamental neuroanatomical organization (dentate gyrus for dummies). *Prog Brain Res* 2007; **163**: 3–22

111. Chen H, Firestein BL. RhoA regulates dendrite branching in hippocampal neurons by decreasing cypin protein levels. *J Neurosci* 2007; **27**: 8378–86
112. Jan YN, Jan LY. Branching out: mechanisms of dendritic arborization. *Nat Rev Neurosci* 2010; **11**: 316–28
113. Obradovic AL, Atluri N, Dalla Massara L, et al. Early exposure to ketamine impairs axonal pruning in developing mouse hippocampus. *Mol Neurobiol* 2017
114. Schwechter B, Rosenmund C, Tolias KF. RasGRF2 RacGEF activity couples NMDA receptor calcium flux to enhanced synaptic transmission. *Proc Natl Acad Sci U S A* 2013; **110**: 14462–7
115. Xiao L, Hu C, Yang W, et al. NMDA receptor couples Rac1-GEF Tiam1 to direct oligodendrocyte precursor cell migration. *Glia* 2013; **61**: 2078–99
116. Murase S, McKay RD. Matrix metalloproteinase-9 regulates survival of neurons in newborn hippocampus. *J Biol Chem* 2012; **287**: 12184–94

Handling editor: H.C. Hemmings Jr